The Influence of Surface Wind Stress over the equatorial Atlantic on Oceanic Upwelling Processes during FGGE 1979

Hans Jürgen PANITZ (1) and Peter SPETH (2)

ABSTRACT

The oceanic response to atmospheric forcing over the equatorial Atlantic Ocean is investigated for the FGGE year 1979. For this purpose local wind and SST measurements and large scale numerical analyses of wind stress and SST are used. The surface meteorology over the tropical Atlantic is described and compared with climatology. The most prominent fluctuations of the wind stress components and the SST, with periods from 4 months to 1 year, are identified using separate EOF analyses. The large scale spatial relationship between the atmosphere and the ocean is studied by combining EOF analyses of the stress components and the SST. The temporal behaviour of the atmospheric and oceanic fluctuations is discussed using a lag correlation analysis of the time coefficients of the separate EOF study. These calculations support the remote forcing theory of the summer upwelling in the Gulf of Guinea. The examination of local wind and SST measurements in the central equatorial Atlantic gives evidence of the passage of an equatorial Kelvin wave, resulting in an upwelling event which is superimposed to the general summer cooling of equatorial SST.

KEY WORDS : Upwelling — Surface wind stress — Equatorial Atlantic — Remote forcing — Sea surface temperature.

RÉSUMÉ

INFLUENCE DE LA TENSION DE VENT DE SURFACE SUR LES PROCESSUS D'UPWELLING DANS L'OCÉAN ATLANTIQUE ÉQUATORIAL, AU COURS DE FGGE 1979

La réponse de l'Océan à l'action de l'atmosphère dans la zone équatoriale de l'Atlantique a été étudiée en 1979, au titre de « FGGE ». A cet effet, des mesures de vent local et de température de surface de la mer sont utilisées. La météorologie à la surface de l'océan est décrite et comparée avec la climatologie. Les composantes les plus importantes de la tension de vent et de la température de surface, de périodes allant de 4 mois à 1 an, sont identifiées à partir d'analyses séparées des fonctions empiriques orthogonales (EOF). La relation spatiale à grande échelle entre atmosphère et océan est étudiée en combinant les analyses des EOF des composantes de la tension de vent et de la température de surface. Les variations dans le temps des conditions atmosphériques et marines sont discutées sur la base de l'analyse des déphasages déduits de l'étude des EOF. Les calculs confirment la théorie du forçage à distance de l'upwelling d'été dans le Golfe de Guinée. L'examen des mesures de vent local et de température de surface dans l'Atlantique central équatorial met en évidence le passage d'une onde de Kelvin équatoriale, engendrant un upwelling qui se superpose au refroidissement général de la température de surface sur l'Équateur pendant l'été.

MOTS-CLÉS : Upwelling — Tension de vent en surface — Atlantique équatorial — Forçage à distance — Température de surface.

(1) *Kernforschungszentrum Karlsruhe, D-7500 Karlsruhe, Federal Republic of Germany.*
(2) *Institut für Geophysik und Meteorologie der Universität zu Köln, Kerpener Strasse 13, D-5000 Köln 41, Federal Republic of Germany.*

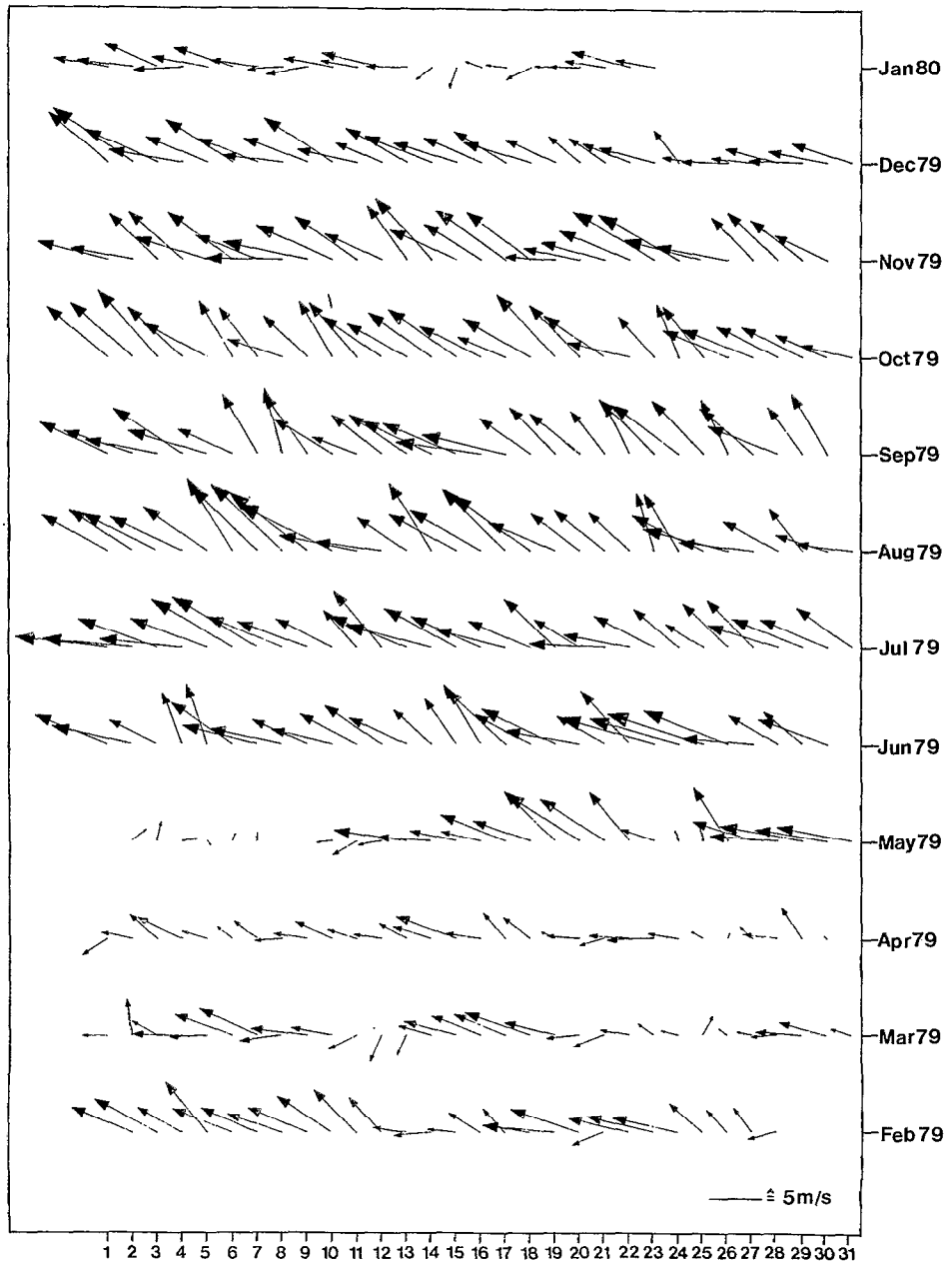

FIG. 1 a.

1. INTRODUCTION

The spatial and temporal variability of the tropical trade wind system determines the climatology of the tropical region between the high pressure belts in both hemispheres. The surface wind stress drives the oceanic circulation, and its variability strongly influences the fluctuations of the equatorial current system and of the sea surface temperature (SST). On the other hand SST anomalies are partly responsible for fluctuations of the tropical atmospheric circulation and they even may influence the weather in extratropical regions by teleconnections.

This paper is only concerned with one direction of the atmospheric-oceanic feedback system. The response of the equatorial Atlantic Ocean on fluctuations of the surface wind stress will be examined for the year 1979 during the First GARP (Global

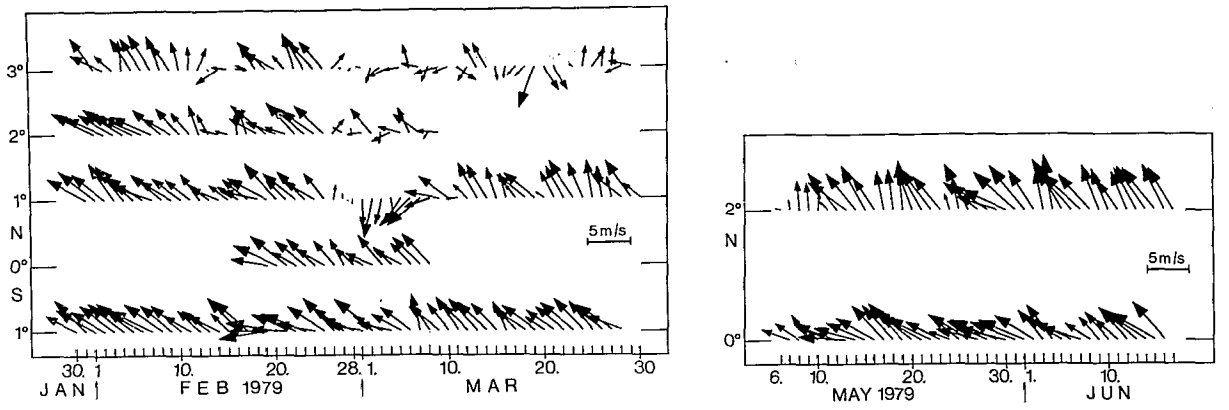

FIG. I b.

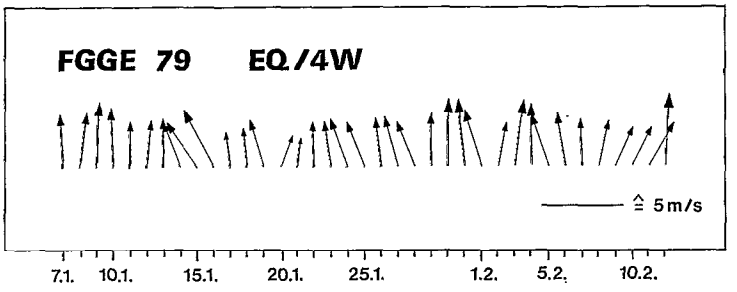

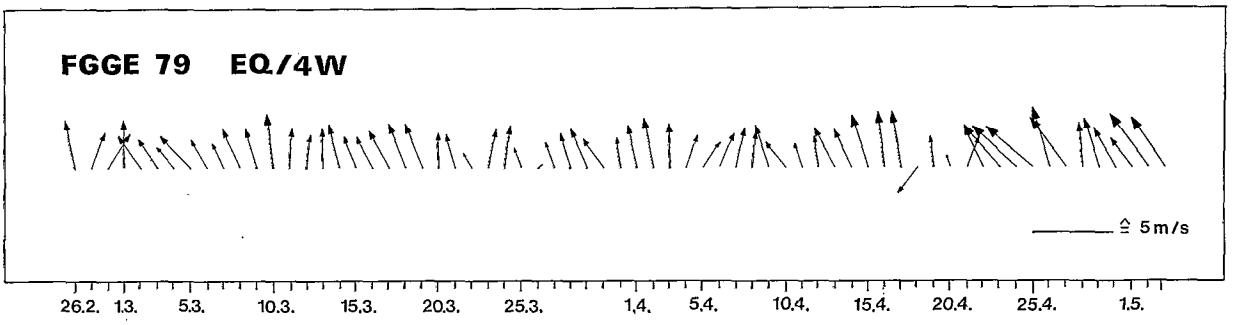

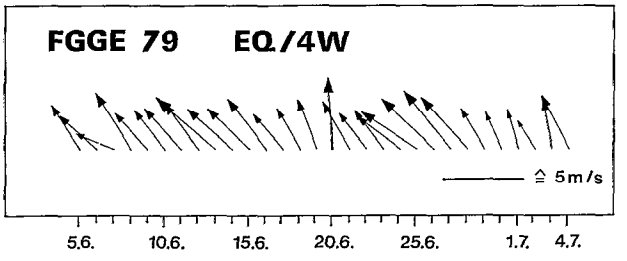

FIG. I c.

FIG. 1. — Daily mean variation of surface wind : a) at St. Peter and St. Paul Rocks, b) at 22° W, c) at the equator for 4° W, a) and b) are from GARZOLI *et al.* (1982). *Variation journalière moyenne du vent de surface: a) aux Rochers St Pierre-St Paul. b) à 22° W, c) à l'Équateur, par 4° W. a) et b) d'après* GARZOLI et al. *(1982)*

TABLE I

Summary of all data used for this study. *Récapitulation de l'ensemble des données utilisées*

	Parameter	Data - Source	Kind of measurement	Measuring Period
a)	local wind measurements along 22°W between 3°N and 1°S during the 51. cruise of RV 'METEOR'	Speth and Panitz (1983)	buoy-measurements	interrupted periods from end of Jan 79 to Jun 79 (see also Table 2)
b)	local measurements of SST along 22° W between 3°N and 1°S during the 51. cruise of RV 'METEOR'	Bauerfeind et al. (1984)	buoy-measurements	a) end of Jan 79 to the end of Mar 79; b) May 79 to Jun 79 (only at the Equator)
c)	local wind measurements at St. Peter and St. Paul Rocks (29°W / 1°N)	Garzoli et al. (1982)	tower measurement	2.2.79 - 23.1.80
d)	local wind measurements in the Gulf of Guinea (EQ / 4°W)	Ch. Colin, ORSTOM, Brest, France (personal communication)	buoy-measurements	three different periods: a) 7.1.79 - 12.2.79 b) 26.2.79 - 3.5.79 c) 5.6.79 - 4.7.79
e)	global SST observations	ECMWF , Reading England	ship and buoy-measurements	Dec 78 - Nov 79
f)	SST observations in the tropical Atlantic	German Weather Service, see Wetteramt, Hamburg F. R. G.	ship and buoy-measurements	Jan 79 - Dec 79
g)	global gridpoint analysis of SST on a 1° square grid	NOAA / NESS, Satellite Data Service, Washington, D. C., U.S.A.	TIROS - N Satellite measurements	1.1.79 - 31.12.79 21 days missing
h)	global gridpoint analysis of zonal and meridional wind components at 1000 hPa on a 1.875° square grid	ECMWF, Reading, England	FGGE Level III_b data set; uninitialized form	1.1.79 - 30.11.79 twice daily

Atmospheric Research Program) Global Experiment (FGGE). An overview of the influence of winds on the oceanic system at the Equator was given by SPETH and PANITZ (1983). MOLINARI *et al.* (1986) presented a synthesis of the near-surface oceanographic and surface meteorological data collected during the FGGE in the Equatorial Atlantic Ocean covering the region between 9 °N and 9 °S.

The data used are described in the second section. Additionally, the mean distributions of surface wind stress and SST together with variances are presented. A comparison of equatorial surface wind speed will be made with the wind analysis of MOLINARI *et al.* (1986, and personal communication) and with the climatology of HASTENRATH and LAMB (1977). A similar comparison will be carried out for the equatorial SST. In section three the spatial and temporal variability of the surface wind stress over the tropical Atlantic from 45° W to 13° E and 7° S to 15° N are described using Empirical Orthogonal Functions (EOF). The same is done with SST in the fourth section. The local oceanic response on wind and wind stress variability is examined in section four. The results will be compared with numerical calculations and other diagnostic studies. Section five concludes the paper with some critical remarks and a summary of the results.

2. DATA

All data used in this study are summarized in Table I. More detailed descriptions of the local measurements mentioned under *a)*, *b)* and *c)* of Table I and of the data handling are given in SPETH and PANITZ (1983), BAUERFEIND *et al.* (1984) and GARZOLI *et al.* (1982). The remaining data sets will be described in this section.

2.1. **Surface Meteorology**

Figure 1 presents daily mean wind vectors in the three different regions over the equatorial Atlantic. Mean values and standard deviations are contained in Table I. Over the western Atlantic (Fig. 1a) the wind increases on May 12, after a period of low wind speed and low directional steadiness (GARZOLI *et al.*, 1982). Over the central Atlantic, from February to March (Fig. 1b) the area north of the equator is strongly influenced by the position of the Intertropical Convergence Zone (ITCZ) and of the surface wind confluence (see Fig. 2). Over the equatorial part of the Gulf of Guinea (Fig. 1c) the prevailing wind direction is from the south. Only during June and July a more south-easterly wind is observed (see also Table II).

TABLE II

Mean values and standard deviations of the local wind measurements during FGGE over the equatorial Atlantic; ū: mean zonal wind component; positive to the east; v̄: mean meridional wind component; positive to the north; |v|: mean scalar wind speed, *not* the magnitude of the mean wind vector; σ: standard deviation. *Valeurs moyennes et déviations standard des mesures de vent local, au cours de FGGE, au-dessus de l'Atlantique équatorial; ū: composante zonale moyenne du vent, positive vers l'Est; v̄: composante méridienne moyenne du vent, positive vers le Nord; |v|: vitesse scalaire moyenne du vent, et* non pas *la longueur du vecteur vent moyen; σ: déviation standard*

Position	measuring Period	record length (hours)	ū	σ_u	v̄	σ_v	|v|	$\sigma_{|v|}$
			(m s^{-1})					
29°W / 1°N (St. Peter a. St. Paul) Rocks	2.2.79 ---- 23.1.80	8507	-4.6	2.3	2.2	2.0	5.5	2.1
22°W / 3°N	1.2.79 ---- 29.3.79	1343	-1.0	1.9	0.9	2.7	3.3	1.5
22°W /2°N$_1$	1.2.79 ---- 9.3.79	867	-2.6	2.0	1.9	2.1	4.0	1.6
22°W / 2°N$_2$	5.5.79 ---- 17.6.79	1037	-2.6	1.9	4.1	1.8	5.2	1.8
22°W /1°N	31.1.79 ---- 30.3.79	1383	-2.5	1.7	1.9	2.7	4.2	1.4
22°W / EQ$_1$	18.2.79 ---- 7.3.79	397	-3.0	1.2	2.4	1.3	4.0	1.3
22°W / EQ$_2$	7.5.79 ---- 16.6.79	970	-4.3	1.3	2.6	1.2	5.2	1.2
22°W / 1°S	30.1.79 ---- 28.3.79	1377	-3.8	1.2	2.6	1.4	4.9	1.0
4°W / EQ	7.1.79 ---- 12.2.79	854	-0.3	1.5	4.5	1.4	4.9	1.1
4°W / EQ	26.2.79 ---- 3.5.79	1590	-1.0	2.0	3.3	1.8	4.2	1.4
4°W / EQ	5.6.79 ---- 4.7.79	707	-3.0	1.5	4.0	1.4	5.3	1.4

The ITCZ is here defined as the belt of the maximum cloudiness and of maximum precipitation, connected with expressed horizontal wind convergence (SADLER, 1975). The mean monthly positions of ITCZ are determined subjectively by KÖHNE and SPETH (1982) using cloud images from the satellite METEOSAT. The ITCZ is not necessarily identical with the confluence region of the south-east and north-east trades which is characterized by a vanishing meridional wind component. The surface wind components are calculated from the data set *h)* of Table I. The methods used will be described later. The mean position of the ITCZ in Figure 2 shows that over the central Atlantic the ITCZ and the wind confluence zone are only 1 to 2 degree latitude apart. Especially in summer this is in contrast to the climatological study of HASTENRATH and LAMB (1978). They find a larger meridional distance. Also the wind confluence zone in 1979 does not migrate as far to the north as in the climatological mean. One can conclude that the south-east trade is weak

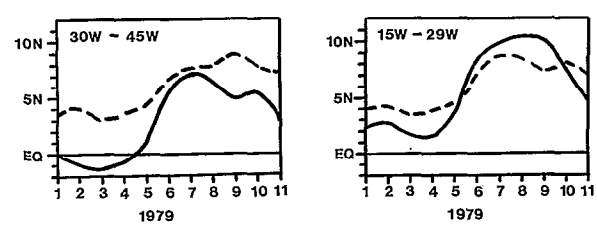

FIG. 2. — Mean monthly position of the ITCZ (solid) and of the surface wind confluence zone (dashed) for the two longitude bands 15° W-29° W and 30° W-45° W. *Position moyenne par mois de l'ITCZ (trait plein) et de la zone de convergence des vents de surface (tireté) pour deux bandes longitudinales, 15° W-29° W et 30° W-45° W*

during the summer of 1979 compared with the climatology. This fact suggests that the equatorial upwelling due to f-divergence might be weaker than normal.

The large scale surface meteorology in the region from 45° W to about 13° E and from 15° N to about 7° S will be studied in this paper examining the surface wind stress. The basis for calculating the surface wind stress is data set *h)* of Table I. Assuming a neutral atmosphere and zero wind at the surface the wind at 10 m height is calculated using a logarithmic windprofile:

$$\Psi_{10} = \Psi_h \frac{\ln\left(\frac{10 + z_o}{z_o}\right)}{\ln\left(\frac{h + z_o}{z_o}\right)}, \quad (1)$$

with the roughness length z_o which is derived by the formula:

$$c_D = \left[\frac{k}{\ln\left(\frac{10 + z_o}{z_o}\right)}\right]^2. \quad (2)$$

Ψ stands for the zonal (u) and meridional (v) wind components. The indices 10 and h indicate a height of 10 m and the geometric height of the 1000 hPa level, respectively. k denotes the v. Karman constant with a value of 0.4. The drag coefficient c_D can be treated as constant for wind speeds less than 10 ms^{-1} (KRISHNAMURTI and KRISHNAMURTI, 1980); a value of $1.4 \cdot 10^{-3}$ is used. From (2) this gives a value of $2.2 \cdot 10^{-4}$ m for z_o.

Daily zonal (τ_x: positive to the east) and meridional (τ_y: positive to the north) wind stress components are calculated from wind components on the 1.875° square grid using the bulk formula:

$$\tau_x = \rho c_D u \mid v_h \mid \quad (3)$$
$$\tau_y = \rho c_D v \mid v_h \mid$$

ρ denotes the density of the air; a value of 1.29 kg m^{-3} is used. $|v_h|$ is the horizontal wind speed.

In Figure 3 mean values of the surface wind stress over the tropical Atlantic for the period January 1979 to November 1979 are shown. Almost the entire region is covered by the north-east and south-east trade wind system. In the Gulf of Guinea the African monsoon has a westerly zonal component; east of 10° W the meridional wind stress dominates and the zonal component nearly vanishes. The zonal wind stress in the equatorial region increases westward. The zone of trade wind confluence slopes from south-west to north-east. The variance of wind stress in Figure 3 shows that the zonal wind stress varies strongly in a region near 8° N/40° W. Other maxima of variance exist off the north-eastern part of Brazil and off Northwest Africa. The weak zonal flow along the West-African coast and over the Gulf of Guinea does hardly vary throughout the year. The meridional wind stress shows the strongest variability off Northwest Africa and off Northeast Brazil. The annual variance in the Northern Hemisphere is stronger than in the southern part of the globe. The reason is the annual migration of the confluence zone which mostly can be found north of the equator.

In Figure 4 mean monthly wind speeds are compared with those of MOLINARI *et al.* (1986, and personal communication) who performed a separate wind analysis on a 2° grid, for which they have used only surface wind observations over the tropical Atlantic. They compare their winds with the climatology of HASTENRATH and LAMB (1977). East of 10° W both analyses for 1979 are in favourable agreement and they are slightly higher than the climatological values. West of 10° W these two analyses show large differences. In the boreal winter and spring the winds used by us are comparable with the climatology. But during the summer they are 1 to 2 ms^{-1} weaker than the climatological average. This is consistent with the relatively southern position of the surface wind confluence zone described above (Fig. 2).

2.2. Sea Surface Temperature

The basis for the SST analyses are daily values of NOAA's (National Oceanic and Atmospheric Administration of USA) National Earth Satellite Surface (NESS), Global Operational Sea Service Temperature Computation (GOSSTCOMP) fields in 1° squares (Table Ig), ship and buoy measurements of SST provided by the European Centre for Medium Range Weather Forecasts (ECMWF) and the German Weather Service (Tables Ie, f) and time series of SST in the central equatorial Atlantic (Table Ib). The latter data set will be discussed in more detail in section 5.

Because the accuracy of satellite-derived SST is affected by many factors (BARNETT *et al.*, 1979) the TIROS-N SST data (Table Ig), which form the basis for GOSSTCOMP analyses, are combined with the ground-truth observations from ships and buoys (Tables Ie, f).

The in-situ observations are from two different sources, and values which appear twice are eliminated: 67460 observations in the region between 45° W and approximately 13° E and between 7° S and 15° N are retained. Table IIIa shows the number of observations per month. The consistency of the observation is tested in the following manner. The region 45° W-15° E, 7° S-15° N is divided into 220 subregions, each 3° longitude by 2° latitude. For each subregion monthly averages and standard

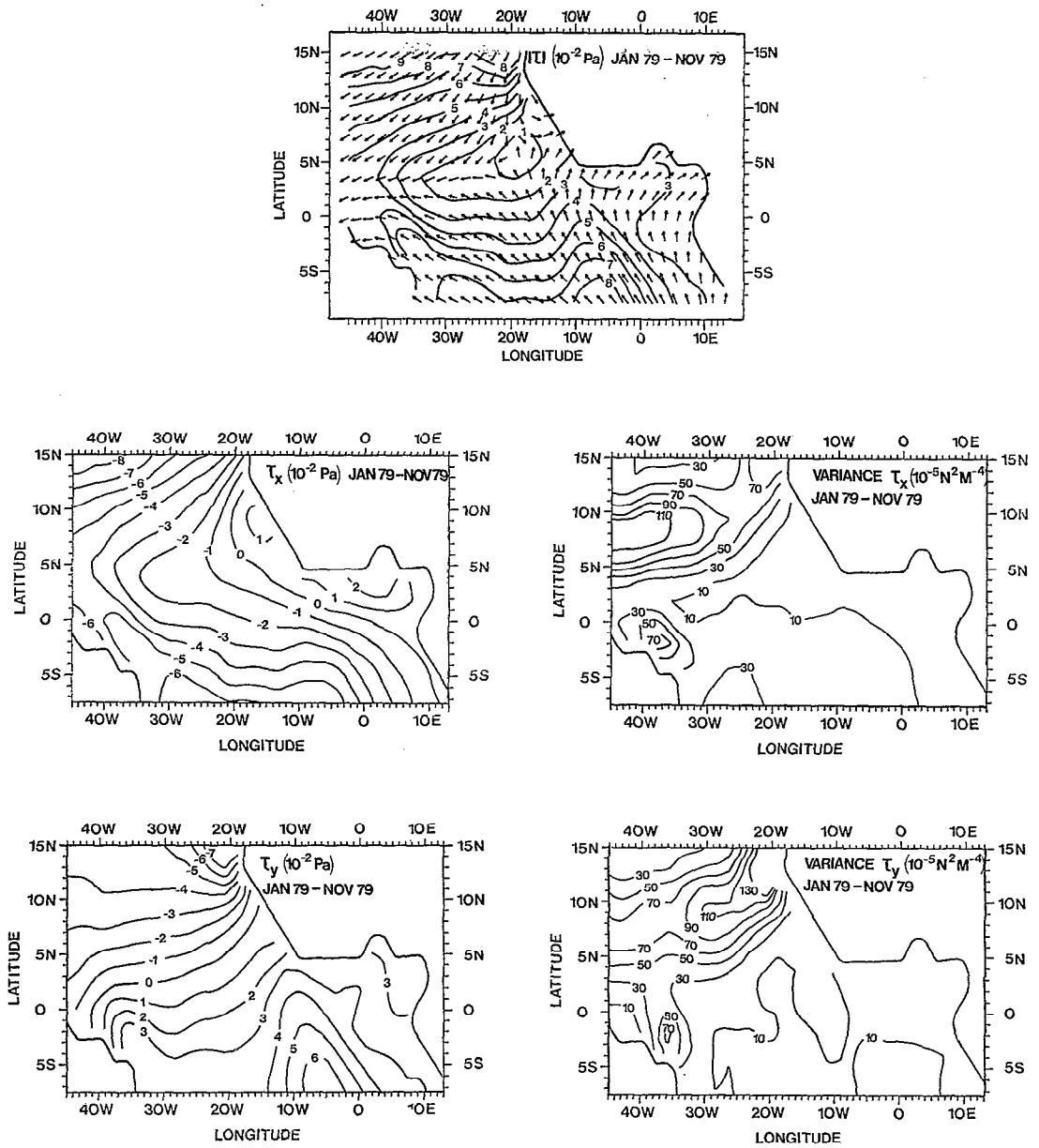

FIG. 3. — Mean wind stress for the period January through November 1979. Top : the direction of stress is indicated by vectors of unit length and the magnitude by contour lines. Middle: mean zonal wind stress (τ_x) and corresponding variance. Bottom: mean meridional wind stress (τ_y) and corresponding variance. Variance is computed from mean monthly data. *Tension moyenne du vent de janvier à novembre 1979. En haut: la direction de la tension est indiquée par des vecteurs de longueur unitaire et l'intensité par des isolignes. Au milieu: tension moyenne du vent zonal (τ_x) et variance correspondante. En bas: tension moyenne du vent méridien (τ_y) et variance correspondante. La variance est calculée à partir des données moyennes mensuelles*

deviations (σ) are calculated. Each observation entering the averaging procedure is weighted by the distance between the observation point and the south-western edge of the subregion. Then the editing procedure described in RASMUSSON and CARPENTER (1982) removes erroneous data. Because the $\pm 3.56\sigma$ limit of Rasmusson and Carpenter is not sufficient to remove all unreasonable data, it is assumed additionally that the difference between the monthly mean and the observation must be less than $\pm$ 4 °C. All data which do not fullfil this second criterium are also removed. In total, 1620 observ-

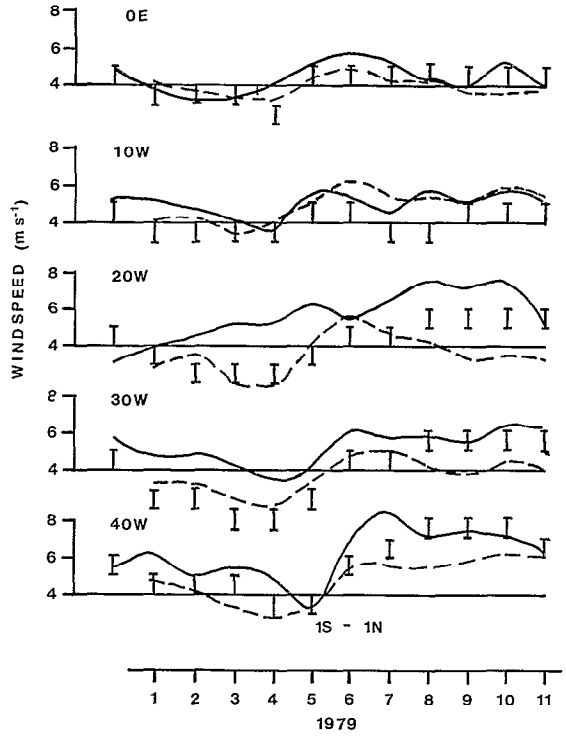

FIG. 4. — Mean monthly wind speed at the equator for different longitudes during 1979. Solid: analysis from MOLINARI *et al.* (1986, and personal communication). Dashed: surface wind from ECMWF, used in this study. Vertical bars: climatology from HASTENRATH and LAMB (1977), corresponding to their contour interval of 1 m s^{-1}. *Vitesse moyenne mensuelle du vent à l'Équateur, en différentes longitudes, en 1979. En trait plein: analyse d'après* MOLINARI et al. *(1984). En tireté: vent de surface d'après ECMWF, utilisé dans la présente étude. Barres verticales: climatologie selon* HASTENRATH *et* LAMB *(1977), correspondant à leur intervalle de 1 m s^{-1}*

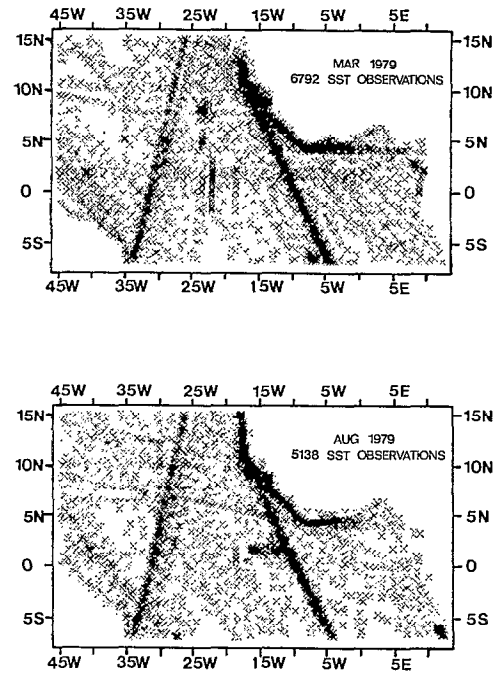

FIG. 5. — Available sea surface temperature observations for March and August 1979. The number of observations is 6792 for March and 5138 for August 1979. *Observations de température de surface disponibles pour mars et août 1979; 6792 observations en mars, 5138 en août*

ations were rejected by this quality test. The number of observations per month after the test is given in Table IIIb.

Most of the observations are concentrated along shipping routes (Fig. 5). From January to June 1979 the number of observations per month generally exceeds 6000, with the largest values (> 7000) in February, May and June, which were the Special Observation Periods of the FGGE. Beginning in July the number of observations decreases with a minimum of 514 observations in December 1979.

To combine the SST observations and the satellite data a five scan correction method analysis, according to CRESSMAN (1959), has been carried out using the daily TIROS-N SST field as the first guess for the first scan. For the following scans the previous scan analysis is used as a first guess. Table IV shows

TABLE III

a: number of SST in-situ observations per month before the data are quality tested. b: number of SST in-situ observations per month after the test. *a: Nombre d'observations de température de surface in situ, par mois, avant application du test de qualité. b: Nombre d'observations de température de surface in situ, par mois, après application du test de qualité*

	Jan	Feb	Mar	Apr	May	Jun	Jul	Aug	Sep	Oct	Nov	Dec
a)	7556	7856	6960	6044	7745	7449	5819	5230	4768	4421	3079	533
b)	7391	7685	6792	5927	7534	7198	5689	5138	4649	4328	2995	514

the values of scan radii and tolerances corresponding to successive scans. After the correction, a first order SHAPIRO (1970) filter is applied in the zonal and meridional directions (*i.e.* a two-dimensional filter) to each of the corrected daily SST fields. The filter eliminates waves with lenghts of $2\Delta x$ (with Δx equal to 1° grid resolution) while leaving long waves nearly unchanged. Gaps in GOSTCOMP fields are interpolated with observations using the method of BARNETT (1977) with the aid of Empirical Orthogonal Functions (EOF). This procedure is described by PANITZ (1984). Finally, the analyses are temporally smoothed by a one-dimensional fourth-order Shapiro filter. By this procedure 365 daily SST analyses (1 January-31 December 1979) in the region from 45° W-13° E and from 7° S-15° N with a grid resolution of 1° square are obtained.

TABLE IV

Values of scan radii and tolerances. *Valeurs des rayons de balayage et tolérances*

Scan Number	Radius (km)	Tolerance (°C)
1	900	5
2	600	4
3	350	3
4	150	2
5	100	2

The mean annual SST distribution (Fig. 6) shows a belt of high temperatures in the central Atlantic. It extends from the African coast towards the western boundary of the basin. A belt of low equatorial SST due to equatorial upwelling cannot be identified. The annual variability of SST is largest in the coastal upwelling areas off Northwest and Southwest Africa. In the central tropical Atlantic the annual variance nearly vanishes. Mean monthly SST distributions (not presented here) show that March 1979 is the month with the highest temperatures and the smallest gradients south of about 7° N, as already pointed out by MOLINARI *et al.* (1986). The highest SST occur in the Gulf of Guinea. The lowest temperatures are observed during March 1979 off the west African coast, where SPETH and KÖHNE (1983) have shown that strong coastal upwelling normally occurs during boreal winter and spring. During August 1979 the cold water in the eastern part of the basin, which first appears in May and then migrates northeastward, covers its maximum area. In August the entire Gulf of Guinea is occupied by anomalously cold water. The low SST extends westward and reaches its most westerly position on the equator at about 25° W.

MOLINARI *et al.* (1986) used research vessel data and merchant ship observations recorded from December 1978 to November 1979 to produce monthly SST fields in the tropical Atlantic on a 2° × 2° grid. They find that the large scale SST patterns for 1979 are very similar to climatology, with the mean monthly difference typically less than 1 °C (Fig. 7). While equatorial cooling events in 1979 commence at approximately the same time as climatological cooling, the summer cooling in the central equatorial Atlantic is less intense during 1979, resulting in anomalously higher temperature. A subjective comparison between our mean monthly SST distributions and the results of MOLINARI *et al.* (1986) shows no significant differences, even though the analysis procedures were somewhat different; our fields seem to be smoother than theirs. Along the equator the mean monthly SST values are not significantly different.

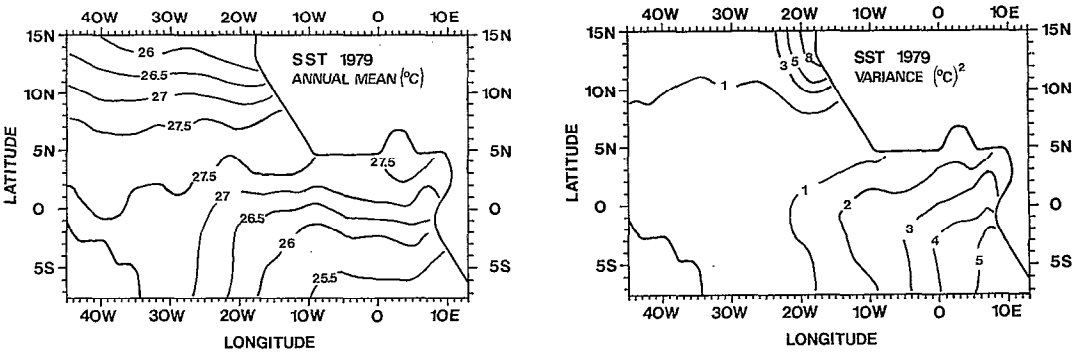

FIG. 6. — Mean annual sea surface temperature for 1979 (left) and variance computed from mean monthly sea surface temperatures (right). *Température de surface moyenne annuelle en 1979 (à gauche) et variance calculée à partir des températures moyennes mensuelles (à droite)*

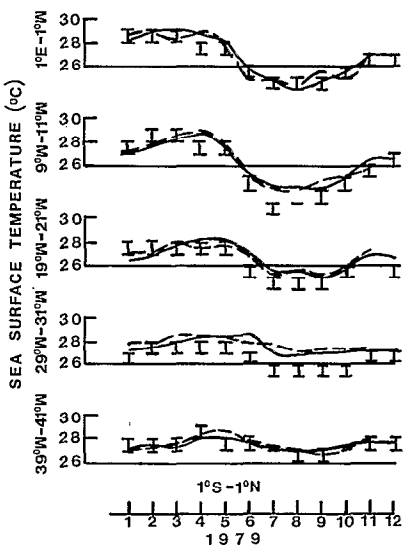

FIG. 7. — Mean monthly sea surface temperatures at the equator (averaged between 1° S and 1° N) for different longitude bands, during 1979. Solid: corrected satellite SST, used in this study. Dashed: SST from MOLINARI *et al.* (1986). Vertical bars: climatology from HASTENRATH and LAMB (1977), corresponding to their contour interval of 1° C. *Températures de surface moyennes mensuelles à l'Équateur (moyenne entre 1° S et 1° N), sur différentes bandes longitudinales, en 1979. En trait plein: températures fournies par satellite, corrigées, utilisées dans la présente étude. En tireté: températures d'après* MOLINARI et al. *(1984). Barres verticales: climatologie selon* HASTENRATH *et* LAMB *(1977), correspondant à leur intervalle de 1 °C*

3. EMPIRICAL ORTHOGONAL FUNCTION ANALYSIS

To analyse the observational data sets Empirical Orthogonal Functions (EOF) are used. For this purpose the observed space and time dependent data are decomposed in the following manner:

$$P(\mathbf{x}, t) = \bar{P}(\mathbf{x}) + \sum_i C_i(t) * U_i(\mathbf{x})$$

where $P(\mathbf{x}, t)$ denotes any time and space dependent parameter (in this paper the parameters are the wind stress components and the SST) and $P(\mathbf{x})$ its time average. $U_i(\mathbf{x})$ denotes the EOF which represents the spatial fluctuations explained by mode i; the principal component $C_i(t)$ describes the temporal behaviour of the spatial EOF. The product $C_i(t)* U_i(\mathbf{x})$ describes the deviation of $P(\mathbf{x}, t)$ from the time mean $\bar{P}(\mathbf{x})$ explained by mode i. In general a few modes will be sufficient to account for the dominating parts of the total spatial and temporal variability of the parameter P. To study the interrelations between several variables it is convenient to consider the normalized departures from the mean for each variable instead of using the actual values. The departures are normalized by the temporal standard deviations. This normalization is a special kind of weighting procedure which is necessary in combined EOF analyses to prevent the first several eigenvectors from being dominated by the variables with largest variances (KUTZBACH, 1967). For a detailed mathematical derivation and description of the physical interpretation of the EOF see for example KUTZBACH (1967).

3.1. Wind Stress

Eigenvectors and principal components are calculated for the normalized daily deviations from the appropriate 334 day mean of zonal and meridional surface wind stress (January 1 through November 30, 1979). Figure 8 shows the percentage part of total variance for the first 17 eigenmodes. According to the test of OVERLAND and PREISENDORFER (1982) these 17 modes are statistically significant, but the quality of such a test strongly depends on the length of the analysed data sets. NORTH *et al.* (1982) calculate statistical errorbars $\delta\lambda_i$ for each eigenvalue λ_i according to the formula

$$\delta\lambda_i = \lambda_i \sqrt{\frac{2}{N}}, \qquad (3)$$

where N denotes the length of the time series. If two neighbouring bars come close together or overlap a physical process is represented by two EOF. NORTH

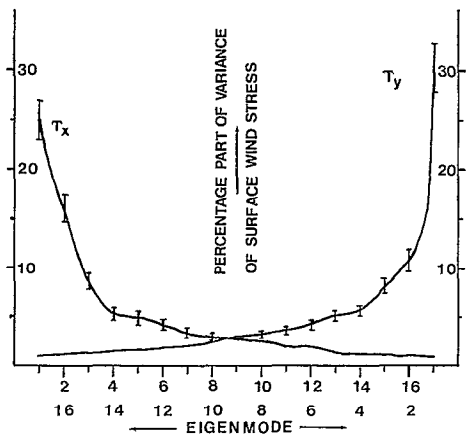

FIG. 8. — Percentage part of variance of zonal (τ_x) and meridional (τ_y) wind stress for the first eigenmodes. Errorbars according to NORTH *et al.* (1982) are added. *Pourcentage de la variance des composantes zonale (τ_x) et méridienne (τ_y) de la tension de vent pour les premiers modes propres. Les barres figurées représentent les intervalles de confiance selon* NORTH et al. *(1982)*

et al. (1982) call this a "degeneracy" of the functions. Only if one errorbar does not overlap another one the appropriate EOF is the single representation of a physical process. According to this criterion only three eigenmodes of each wind stress component can be interpreted physically (Fig. 8). Altogether the first three functions explain 49.7 % and 49.5 % of the variance of the zonal and meridional wind stress component, respectively.

For an investigation of the oceanic response to atmospheric forcing we will use in section 5 the first two EOF of both wind components, which are shown in Figures 9 and 10. The first EOF of the zonal wind stress U_1 (Figure 9 top) explains 25 % of the variance and has a north-south asymmetry, i.e. positive departures in the north are accompanied by negative departures in the south and vice versa. Maximum fluctuations are found in the central regions of both trade wind systems. The time dependent principal component $C_{U1}(t)$ shows that maximum departures occur during February to March and June 1979. From January to mid-May the zonal wind stress north of about 2° N is stronger than the average because $C_{u1} \cdot U_1$ gives a negative departure from a negative mean value; south of 2° N τ_x is weaker. From Mid-May until the end of November 1979 the conditions are reversed. It is noteworthy that the large increase of C_{U1} from mid-May to June 1979 corresponds to a rapid increase of the zonal wind stress along and south of the equator in the central and western Atlantic. We conclude that the first EOF of the zonal wind stress describes the annual fluctuation of the trade winds: predominance of τ_x of the north-east (south-east) trades during Northern (Southern) Hemisphere winter and spring. The annual cycle contains a rapid and strong increase of τ_x in the central and western equatorial Atlantic. Such a sudden onset of zonal wind stress possibly is responsible for the generation of equatorial currents (PHILANDER and PACANOWSKI, 1980) and probably causes summer upwelling in the Gulf of Guinea (MOORE *et al.*, 1978; SERVAIN *et al.*, 1982).

The second EOF of the zonal wind stress (Figure 9 bottom), explaining 16.2 % of the variance, shows

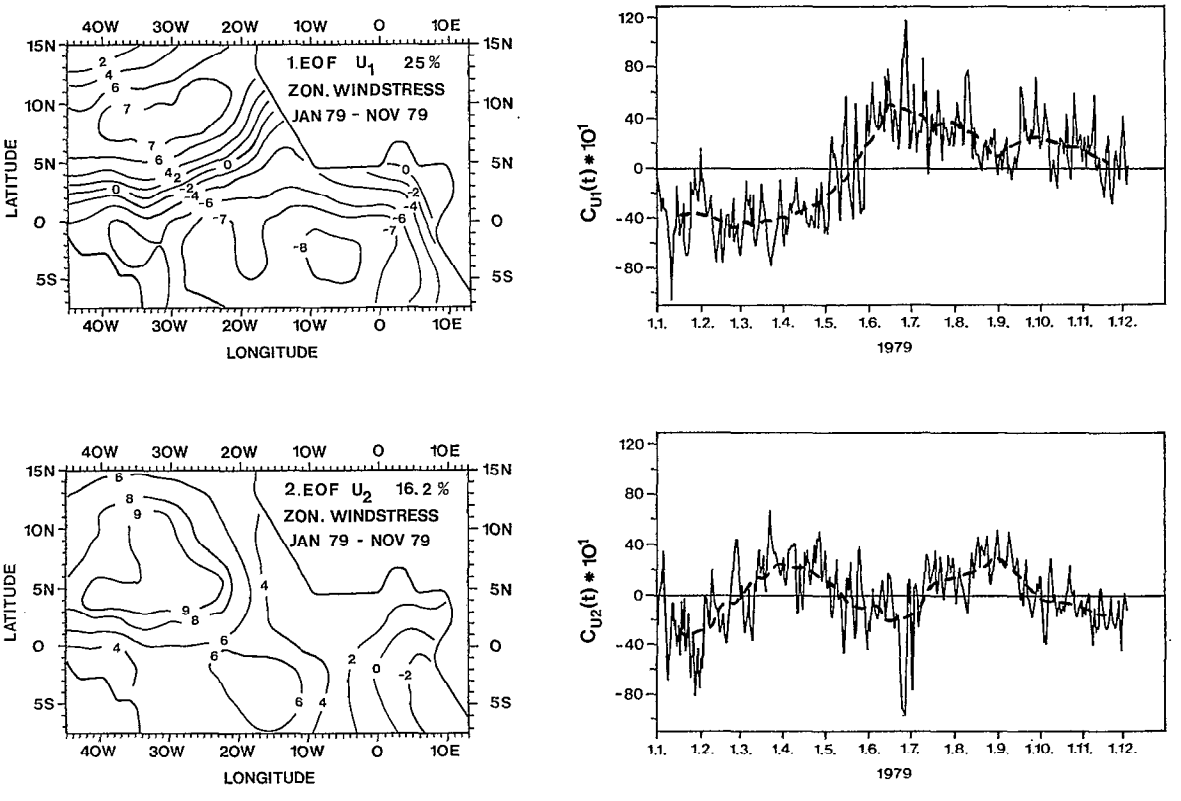

FIG. 9. — *First and second EOF of the zonal wind stress (left), denoted by U_1 and U_2, respectively, and corresponding principal components (right) denoted by C_{u1} and C_{u2}. 31 day overlapping mean values of principal components are dashed. Première (U_1) et seconde (U_2) fonction empirique orthogonale de la composante zonale de la tension de vent (à gauche), et leurs composantes principales correspondantes (C_{u1} et C_{u2}, respectivement) (à droite). La courbe en tireté représente le signal filtré à 31 jours*

in-phase fluctuations over most of the tropical Atlantic. This EOF pattern which is interpreted as a modulation of the annual cycle described by the first EOF extends the area of maximum departures of north-east trades. The maximum in the south-east trade area is shifted westward. Together with its time dependent principal component, the second EOF represents an amplification or damping of the fluctuations described by the first EOF. For example, during May to June the strenghtening of τ_x in the south-east trades is amplified, while the positive departures in the north are reduced. Thus, the rapid increase of easterly zonal wind stress along the equator in the western Atlantic during May to June is caused not only by the annual cycle of τ_x but also by fluctuations with time scales shorter than the annual cycle.

The first EOF of the meridional wind stress V_1 (Figure 10 top), which contains 30.3 % of the variance, represents an in-phase fluctuation throughout the entire area. The amplitude function C_{V1} shows that the principal pattern describes the annual cycle. From January to mid-May 1979 the meridional wind stress is weaker than the average south of the trace wind confluence zone; afterwards, until the end of November, it is stronger. The opposite pattern occurred north of the confluence zone. Extreme values of departures occur in March and from June to August. Principally, amplitude functions for the meridional wind stress of the first EOF are similar to the corresponding functions of the zonal wind stress. After a common increase beginning in May they reach their maximum values in June. Afterwards the coefficient of τ_x decreases slowly. In contrast to this the coefficient of τ_y nearly remains constant until August. This has the consequence that the meridional wind stress of the south-east trade is anomalously strong for nearly two months during summer. It will be shown later that this behaviour forces a SST decrease until September.

In the equatorial region the increase of meridional wind stress occurring in May results in a decrease of SST due to increased f-divergence, which is a large-scale phenomenon depending on the strength of the south-east trade wind. On the other hand, PHILANDER and PACANOWSKI (1981a) attribute SST varia-

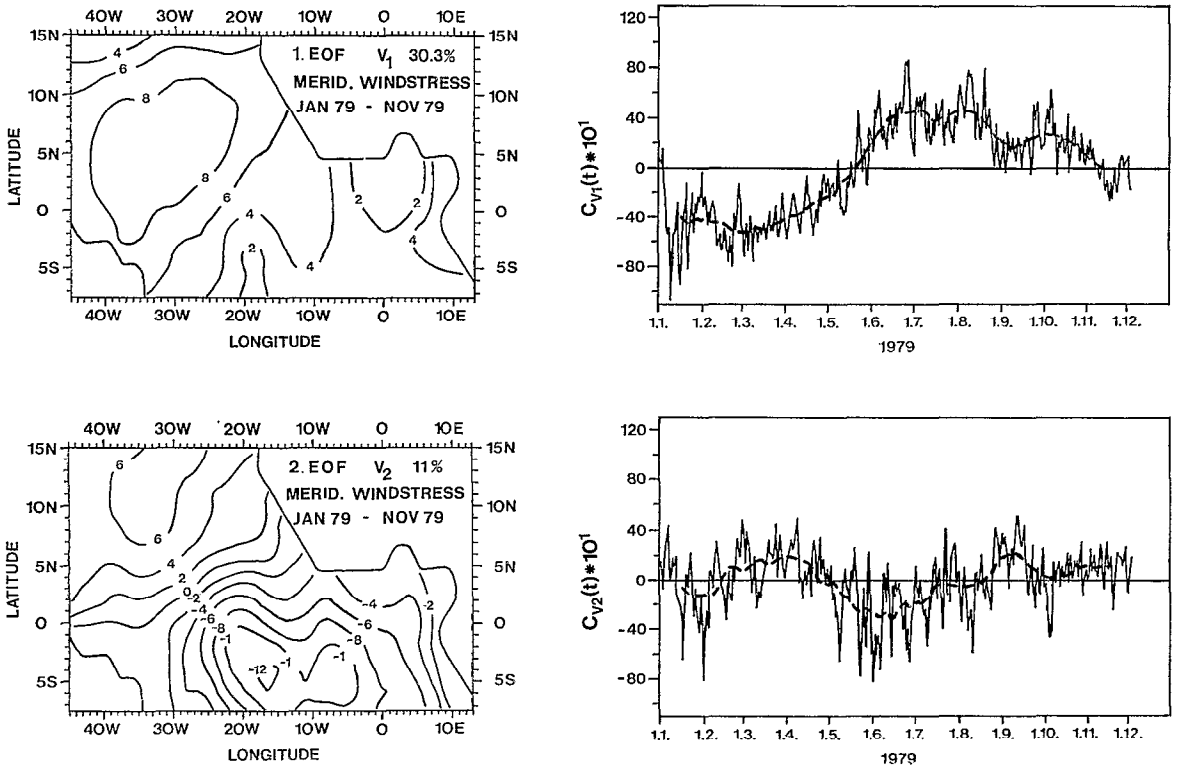

FIG. 10. — First and second EOF of the meridional wind stress (left), denoted by V_1 and V_2, respectively, and corresponding principal components (right) denoted by C_{V1} and C_{V2}. 31 day overlapping mean values of principal components are dashed. *Première (V_1) et seconde (V_2) fonction empirique orthogonale de la composante méridienne de la tension de vent (à gauche) et leurs composantes principales correspondantes (C_{V1} et C_{V2}, respectivement) (à droite). La courbe en tireté représente le signal filtré à 31 jours*

bility in the eastern equatorial Atlantic to fluctuating meridional winds with a period between 50 and 200 days. The time history of the second EOF of τ_y (Figure 10 bottom) which explains 11 % of the variance describes these fluctuations with a period of about 4 to 5 months. The spatial pattern of the second EOF of τ_y shows that the maximum fluctuation occurs in the central and eastern equatorial Atlantic.

3.2. Sea Surface Temperature

Similar to section 3 Empirical Orthogonal Functions are determined for SST. Figure 11s hows the percentage part of total variance for the first seven eigenmodes which are calculated from the daily deviations from the annual mean. These seven modes are significant according to the Overland and Preisendorfer test. Altogether they explain more than 90 % of the variance. It can also be seen from the errorbars, that only the first and second EOF are not degenerated (North *et al.*, 1982).

The first function (Fig. 12 top) contains 64.2 % of the variance. It represents the annual variability of SST. The spatial pattern shows a north-south asymmetry, which means that the SST fluctuations on both sides of the zero contour line are out of phase. This line is nearly identical with the oceanic thermal equator (Molinari *et al.*, 1984). From January to June the SST south of the thermal

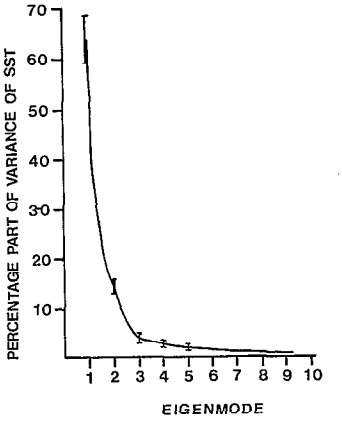

Fig. 11. — Percentage part of the variance of sea surface temperature for the first 9 eigenmodes. Errorbars according to North *et al.* (1982) are added. *Pourcentage de la variance de la température de surface pour les 9 premiers modes propres. Les barres figurées représentent les intervalles de confiance selon* North et al. *(1982)*

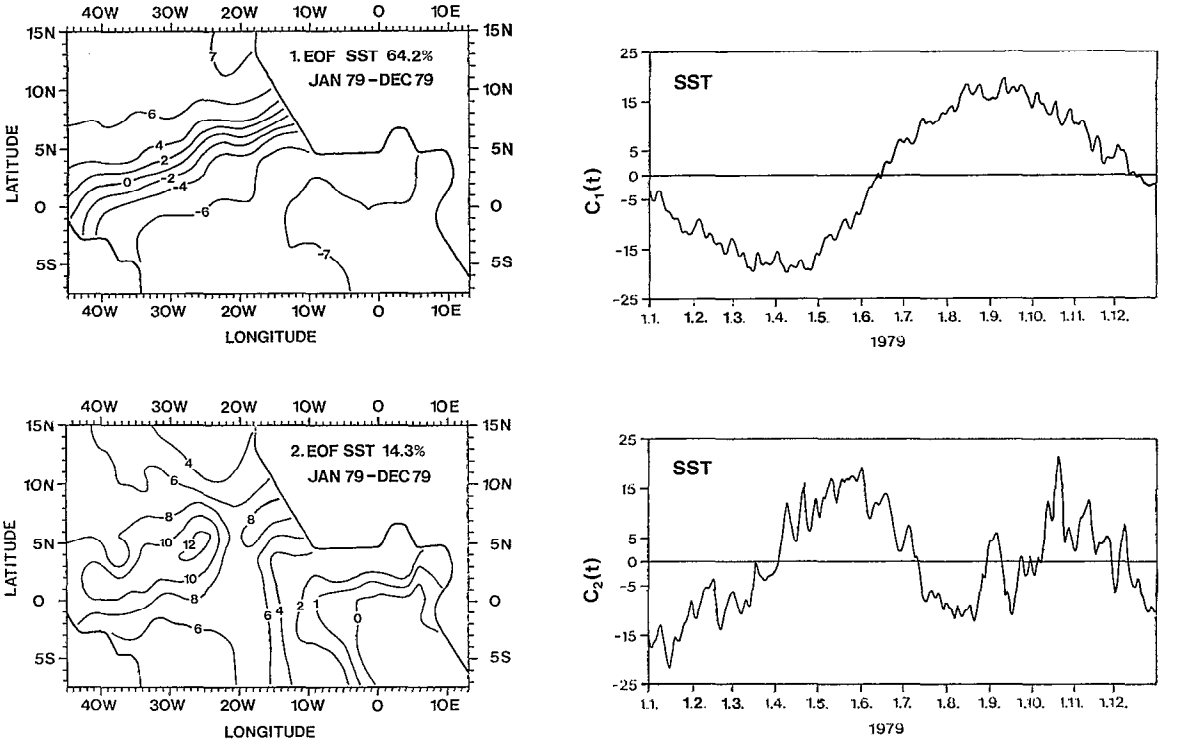

Fig. 12. — First and second empirical orthogonal function of sea surface temperature (left) and corresponding principal components. *Première et seconde fonction empirique orthogonale de la température de surface (à gauche) et leurs composantes principales correspondantes*

equator is relatively high while it is lower than normal from June to November. The opposite holds true for the northern part. Maximum departures appear in the upwelling region off Northwest Africa with coldest water during March/April and in the Gulf of Guinea with coldest water during August/September.

The second EOF (14.3 % of variance, Figure 12 bottom) describes a quasi semi-annual variability of SST which is in phase nearly over the entire equatorial Atlantic. Fluctuations in the region of the thermal equator dominate. From January to March and from July to September negative departures can be observed. They are interrupted by a positive anomaly at the beginning of September. From April to July and from October to November the water is warmer than normal.

3.3. **Combined Analysis**

The large scale relationships between the wind stress variability and the SST fluctuations are studied for the equatorial belt between 5° N and 5° S using the EOF method. The spatial correlation is examined by two combined EOF analyses between τ_x and SST and τ_y and SST. The eigenvectors are calculated for normalized daily deviations from the appropriate 334 day means (January 1 through November 30, 1979).

Figure 13 left shows the first two eigenvectors of the combined analysis between τ_x and SST. Together they explain about 59 % of the variance. The first function mainly reveals two centers of zonal wind stress variability near the equator over the western Atlantic and over the Gulf of Guinea. They are positively correlated with SST fluctuations south of the oceanic thermal equator. Maximum correlation exists between the zonal stress component over the western region and the SST in the Gulf of Guinea. It can be seen from the second function of the τ_x-SST analysis that atmospheric fluctuations in a large region over the central equatorial Atlantic are out of phase with the SST variability along the thermal equator. The same is valid for the second function of the τ_y-SST relationship (Figure 13 right) except that the fluctuations are positively correlated. Both spatial patterns for the second EOF only show very weak or zero correlation over the Gulf of Guinea.

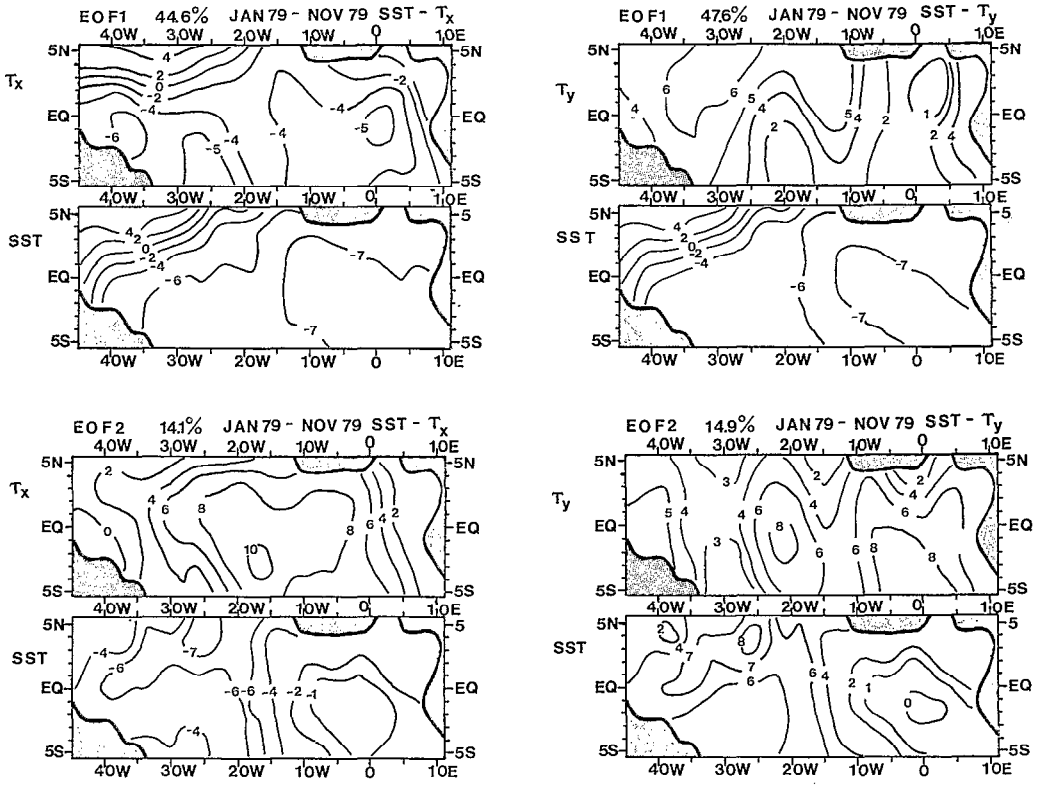

FIG. 13. — Left: First two empirical orthogonal functions of the combined analysis between the zonal wind stress (τ_x) and sea surface temperature (SST). Right: As left, but for meridional wind stress (τ_y) and SST. *A gauche: deux premières fonctions empiriques orthogonales de l'analyse combinée entre la composante zonale de la tension de vent (τ_x) et la température de surface (SST). A droite: id. pour la composante méridienne de la tension de vent (τ_y) et la température de surface (SST)*

TABLE V

Lag-correlations between the time dependent coefficients discussed in sections 3 and 4. Only those correlations are given which are significant at the 95 % level. See text for further explanation. *Corrélations à termes déphasés entre les coefficients dépendant du temps traités dans les parties 3 et 4. Sont seules mentionnées les corrélations significatives au seuil de 95 %. Voir texte pour plus ample information*

	C_{U1}	C_{U2}
SST_1	.91 27 C_{U1}	/
SST_2	.61 40 SST_2	.62 45 C_{U2}

	C_{V1}	C_{V2}
SST_1	.94 25 C_{V1}	.60 70 SST_1
SST_2	.60 45 SST_2	.63 55 C_{V2}

This is also the case between the meridional wind stress and the SST described by the first eigenvector.

The combined analysis has shown that the centers of both wind stress and SST variability, as well as those from the separate analyses are spatially correlated in the equatorial region, because the patterns of Figures 9, 10 and 11 are similar to those of Figure 13. By that reason it seems justified to get insight into the temporal relationship between atmospheric and oceanic fluctuations by considering the lag-correlations between the 1-month-running means of the time coefficients of the EOF's discussed in sections 3.1 and 3.2 The 1-month-running means (Fig. 14) are chosen to eliminate high frequency fluctuations. The first lines of Table V give the correlation between corresponding time coefficients. The second lines define the temporal lag while the third indicate the leading parameters. Only those correlations are considered which are significant at

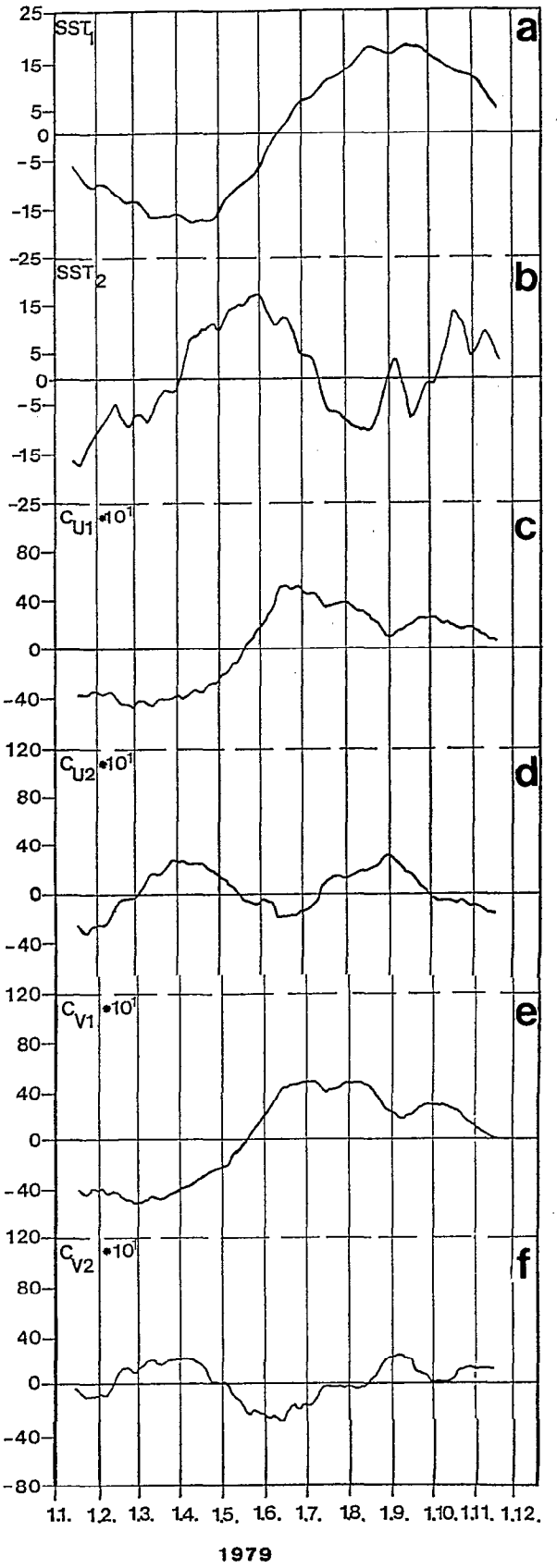

→

FIG. 14. — Time dependent coefficients for the empirical orthogonal functions discussed in sections 3 and 4. Represented are 31 day overlapping mean values. The following coefficients are represented; a: the first EOF of SST; b: the second EOF of SST; c: the first EOF for zonal wind stress; d: the second EOF for zonal wind stress; e: the first EOF for meridional wind stress; f: the second EOF for meridional wind stress. *Coefficients de temps pour les fonctions empiriques orthogonales discutées dans les parties 3 et 4. Est représenté le signal filtré à 31 jours. Les coefficients sont représentés; a: la première fonction empirique orthogonale de la température de surface; b: la seconde fonction empirique orthogonale de la température de surface; c: la première fonction empirique orthogonale de la composante zonale de la tension de vent; d: la seconde fonction empirique orthogonale de la composante zonale de la tension de vent; e: la première fonction empirique orthogonale de la composante méridienne de la tension de vent; f: la seconde fonction empirique orthogonale de la composante méridienne de la tension de vent*

the 95 % level according to the t-test of Student. It can be seen from Table V that the time coefficients of the first EOF's of all parameters are highly correlated. The atmospheric fluctuations lead the SST by about 25 to 27 days. This means that the positive spatial correlation between the wind stress components and the SST discussed above in Figure 13 have a temporal lag of about 1 month. For example, the strengthening of the wind stress especially over the western part of the Atlantic near 40° W in May is followed by a decrease of SST in the Gulf of Guinea one month later. This result confirms the remote forcing theory of the coastal upwelling in the Gulf of Guinea by MOORE *et al.* (1978) which already got observational evidence by SERVAIN *et al.* (1982). But it is not only the increase of the zonal wind stress component which is responsible for the upwelling process. Quantitatively the fluctuations of the meridional component over the western Atlantic are of the same order as those of the zonal component (Fig. 13 top right). It is also evident, that the SST anomaly increases until August/September (Fig. 14a) although the zonal wind stress already decreases since July (Fig. 14c). In contrast to this behaviour of the zonal component the strong positive anomaly of the meridional wind stress persists (Fig. 14e) and forces the increase of negative SST anomaly. This SST deviation reaches its maximum in August. Nearly at the same time the meridional wind stress also weakens again.

Further correlations which indicate an atmospheric forcing of oceanic fluctuations exist between the principal components of the second EOF (Table V). The orthogonal functions describe spatial relationships between both wind stress components over the central Atlantic and the SST variability along the oceanic thermal equator. The 4 to 5 months variations of the atmospheric parameters lead the semi-annual SST fluctuation by about 1.5 to 2 months (Table V, Fig. 14).

4. LOCAL OCEANIC RESPONSE TO ATMOSPHERIC FORCING AT 22° W

Hourly averages of SST at the equator and at 1° N which are calculated from the data set *b)* of Table I show two cooling processes (Fig. 15). The first one, from February 17 to February 26, interrupts a period of general SST warming (Fig. 16). PHILANDER (1981) shows that the large scale SST increase is caused by a general relaxation of the trade-wind system (Fig. 1a, b). Using spectral analysis no local relationship between the wind variability and the SST fluctuations can be found (SPETH and PANITZ, 1983). According to a study of FAHRBACH (1983) the reason for the cooling in February is one single event

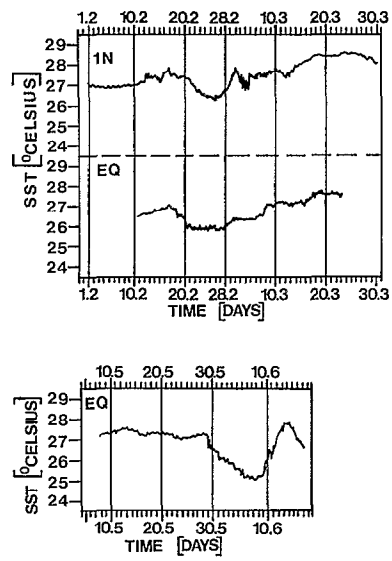

FIG. 15. — Hourly averages of sea surface temperatures at the equator and 1° N from 1 February 1979 to 30 March 1979 (top) and at the equator from 8 May 1979 to 18 June 1979 (bottom). Values are for 22° W. *Température moyenne horaire de l'Équateur et à 1° N, du 1er février au 30 mars 1979 (en haut), et à l'Équateur, du 8 mai au 18 juin 1979 (en bas). Valeurs enregistrées par 22° W*

of increasing wind. The strengthening wind causes a meridional divergence of water. Maximum correlation between the divergence and equatorial temperature fluctuations occur with a lag of 2-4 days. FAHRBACH (1983) calculates an upwelling velocity of (3.3 ± 2.1) m/d, which is the representative value of the equatorial summer upwelling. The time of minimum SST in February coincides with the time of maximum upwelling velocity. The cooling event is not detectable in the daily averages of large-scale satellite derived SST time series (Fig. 16). This fact confirms the local character of the upwelling event in February.

In May a slow SST decrease can be observed starting on May 12. At the same time the wind reinforces as well over the central equatorial Atlantic at 22° W as over the western Atlantic (Fig. 1a, b). Inspecting the first EOF (Fig. 9 top and Fig. 10 top) at the same time both wind stress components become stronger than the annual mean. The spatial EOF pattern of the zonal wind stress shows maximum departures over the central equatorial Atlantic extending westward to approximately 40° W. According to model calculations of PHILANDER and PACANOWSKI (1980) it is such a sudden increase of the wind stress which drives the eastward propagation of equatorial Kelvin waves. At the same time a westward oceanic surface current linearly intensifies

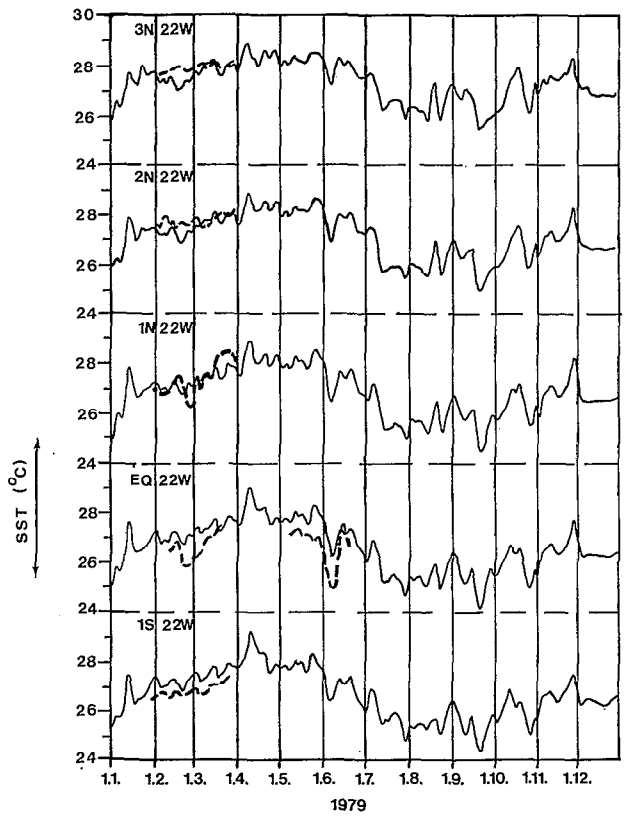

FIG. 16. — Daily sea surface temperatures at 22° W between 1° S and 3° N for January through December 1979. Dashed are buoy data (dataset b from Table 1), and solid are corrected satellite data (section 2.2). *Température journalière de surface par 22° W, entre 1° S et 3° N, de janvier à décembre 1979. En tireté, les données de bouée (jeu de valeurs du cadre b du tableau I), en trait plein, les données satellitaires corrigées (partie 2.2)*

along the equator. With the arrival of the Kelvin wave at a special place the acceleration of the current stops. According to the model it is the second baroclinic Kelvin mode which causes the oceanic fluctuations. The velocity of the wave is 1.4 m/s (MOORE and PHILANDER, 1977). Assuming the source region of the wave at 40° W the wave needs about 17 days to reach 22° W. On May 29, 17 days after the onset of wind intensifications and SST decrease, a strong cooling event is observed at 22° W (Fig. 13), which indicates the arrival of the wave. The SST reaches a minimum on June 6/7, and then quickly increases again. FAHRBACH (1983) observes the arrival of the Kelvin wave on June 2. He uses measured surface current data to verify the nearly linear development of a westward current. But he assumes that the source region of the Kelvin waves is situated near the western coast of the Atlantic at 45° W. In this paper a source region near 40° W is assumed. The wave needs 4-5 days to travel from 45° W to 40° W. This explains the different arrival times of the wave at 22° W. The daily averages of satellite derived SST (Fig. 16) also show the upwelling event with a decreasing amplitude north of the equator. This meridionally decreasing upwelling intensity is also a hint to the passage of the Kelvin wave.

5. CONCLUSION

In this paper the oceanic response in the equatorial Atlantic on the atmospheric forcing has been studied for the FGGE year 1979. For this purpose surface registrations and large scale grid point analyses of wind and SST have been analysed. EOF analyses of the wind stress components and the SST identify the most prominent fluctuations with periods from 4 months to 1 year. The annual variability of SST lags the atmospheric annual fluctuations by about 1 month. The SST reacts with an increase to the relaxation of wind stress and vice versa. The ocean's response dominates in the eastern part of the equatorial Atlantic. A sudden increase of both wind stress components over the western Atlantic in May gives the impulse for the oceanic summer cooling. A positive anomaly of the meridional wind stress with a 2-months duration from June to August forces a continuous decrease of SST until the end of August.

A semi-annual variability of SST in the region of the oceanic thermal equator is correlated with the 4 to 5 months variations of the wind stress components over the central part of the Atlantic. Positive SST anomalies in spring and late autumn appear 1.5 to 2 months later than anomalously weak winds.

Using local buoy measurements of SST and wind a possible local forcing of two upwelling events in the central equatorial Atlantic has been discussed. The first cooling event appears in February and it is superimposed to a general warming of the SST. Using spectral analysis no evidence for a local forcing can be found while FAHRBACH (1983) shows that a single local event of increasing wind is responsible for the SST decrease. At the end of May the second upwelling event is observed. It is due to the passage of an equatorial Kelvin wave, induced in the western Atlantic near 40° W by the sudden increase of the wind. The wave propagates eastward with a velocity of about 1.4 m/s.

Compared to climatology the trade wind system of the FGGE year 1979 is anomalously weak. This is shown by studying the ITCZ positions during the year. The convergence zone does not migrate as far to the north in summer as in the climatological mean.

By that reason the equatorial cooling of SST is also weaker than the climatological average although it starts nearly at the same time as in the long terms average.

From Table V it can be seen that there also exist correlations between the time coefficients of the first SST function and the second function of the meridional wind stress and between the time amplitude of the second SST function and the first eigenvector of the zonal wind stress. In both cases the oceanic variability leads the atmospheric one. We have not discussed these results because it was not the aim of this study to investigate the oceanic influence on the atmosphere. It was our goal to verify existing theories of the atmospheric influence on SST variability, especially the remote forcing theory of the summer upwelling in the Gulf of Guinea.

Manuscrit accepté par le Comité de Rédaction le 15 janvier 1987 et reçu au Service des Éditions le 21 avril 1987.

REFERENCES

BARNETT (T. P.), 1977. — The principal time and space scales of the Pacific trade wind field. *J. Atmos. Sci.*, 34: 211-236.

BARNETT (T. P.), PATZERT (W. C.), WEBB (S. C.) and BEAN (B. R.), 1979. — Climatological usefullness of satellite determined sea surface temperatures in the tropical Pacific. *Bull. Am. Met. Soc.*, 60: 187-205.

BAUERFEIND (E.), BROCKMANN (C.), FAHRBACH (E.), MEINCKE (J.), PANITZ (H.-J.), ROHARDT (G.) and SY (A.), 1984. — A compendium of the oceanographic data measurement during "FGGE-Equator '79", Cruise No. 51 of R.V. METEOR. METEOR Forschungsergebnisse.

CRESSMAN (G. P.), 1959. — An operational objective analysis system. *Mon. Wea. Rev.*, 87 : 367-474.

FAHRBACH (E.), 1983. — Transportprozesse im zentralen äquatorialen Atlantik und ihr Einfluß auf den Wärmeinhalt. *Bericht aus dem Inst. f. Meerreskunde*, Kiel, Nr. 113, 140 pp.

GARZOLI (S. L.), KATZ (E. J.), PANITZ (H.-J.) and SPETH (P.), 1982. — In situ wind measurements in the equatorial Atlantic during 1979. *Oceanol. Acta*, 5: 281-288.

HALTINER (G. J.), 1971. — Numerical Weather Prediction. John Wiley & Sons, Inc., New York, 317 pp.

HASTENRATH (S.) and LAMB (P.), 1977. — Climatic Atlas of the tropical Atlantic and western Pacific ocean. University of Wisconsin Press, 112 pp.

HASTENRATH (S.) and LAMB (P.), 1978. — On the dynamics and climatology of surface flow over the equatorial oceans. *Tellus*, 30 : 436-448.

KÖHNE (A.) and SPETH (P.), 1982. — Variation of the ITCZ in the Atlantic during FGGE. Tropical Ocean-Atmosphere Newsletter, No. 9.

KRISHNAMURTI (T. N.) and KRISHNAMURTI (R.), 1980. — Surface meteorology over the GATE A-Scale. *Deep Sea Res.* Vol. 26, Suppl. II, Part A : 26-61.

KUTZBACH (J. E.), 1967. — Empirical eigenvectors of sea level pressure, surface temperature and precipitation complexes over North America. *J. Appl. Meteor.*, 6 : 791-802.

MOLINARI (R. L.), GARZOLI (S. L.), KATZ (E. J.), HARRISON (D. E.), RICHARDSON (P. L.) and REVERDIN (G.), 1986. — A synthesis of the First GARP Global Experiment (FGGE) in the Equatorial Atlantic Ocean. *Prog. Oceanogr.* 16 : 91-112.

MOORE (D. W.) and PHILANDER (S. G. H.), 1977. — Modelling the tropical ocean circulation. *In:* The Sea, Vol. 6, John Wiley & Sons, New York : 319-361.

MOORE (D. W.), HISARD (P.), MC CREARY (J.), MERLE (J.), O'BRIEN (J. J.), PICAUT (J.), VERSTRAETE (J. M.) and WUNSCH (C.), 1978 : Equatorial adjustment in the eastern Atlantic. *Geophys. Res. Lett.*, 5 : 637-640.

NORTH (G. R.), BELL (T. C.), CALAHAR (R. F.) and MOENG (F. J.), 1982. — Sampling errors in the estimation of empirical orthogonal functions. *Mon. Wea. Rev.*, 110 : 699-706.

OVERLAND (J. E.) and PREISENDORFER (R. W.), 1982. — A significance test of principal components applied to a cyclone climatology. *Mon. Wea. Rev.*, 110 : 1-4.

PANITZ (H. J.), 1984. — Einfluß der bodennahen Windschubspannung über dem äquatorialen Auftrieb und den Auftrieb im Golf von Guinea während FGGE 1979. Dissertation Köln.

PHILANDER (S. G. H.) and PACANOWSKI (R. C.), 1980. — The generation of equatorial currents. *J. Geophys. Res.*, 86, C3 : 1903-1916.

PHILANDER (S. G. H.) and PACANOWSKI (R. C.), 1981a. — The oceanic response to cross equatorial winds (with application to coastal upwelling in low latitudes). *Tellus*, 33 : 204-210.

PHILANDER (S. G. H.), 1981. — The response of equatorial oceans to a relaxation of the trade winds. *J. Phys. Ocean.*, 11 : 176-189.

RASMUSSON (E.) and CARPENTER (T.), 1982. — Variation in tropical sea surface temperature and surface wind fields associated with the Southern Oscillation/El Nino. *Mon. Wea. Rev.*, 110 : 354-384.

SADLER (J. C.), 1975. — The monsoon circulation and cloudiness over the GATE area. *Mon. Wea. Rev.*, 103 : 369-387.

SERVAIN (J.), PICAUT (J.) and MERLE (J.), 1982. — Evidence of remote forcing in the equatorial Atlantic Ocean. *J. Phys. Ocean.*, 12 : 457-463.

SHAPIRO (R.), 1970. — Smoothing, filtering and boundary effects. *Rev. Geophys. Space Phys.*, 8 : 359-387.

SPETH (P.) and KÖHNE (A.), 1983. — The relationship between sea surface temperature and wind off Northwest Africa and Portugal. *Oceanogr. Trop.*, 18 (1) : 68-80.

SPETH (P.) and PANITZ (H.-J.), 1983. — The variability of local winds at 22° W and their influence on the oceanic system at the Equator in the Atlantic during FGGE. *In:* J. C. J. Nihoul (Editor): Hydrodynamics of the Equatorial Ocean : 51-64, Elsevier Science Publishers B.V., Amsterdam.